IOP Publishing Journal of Physics: Condensed Matter
J. Phys.: Condens. Matter **32** (2020) 145301 (9pp) https://doi.org/10.1088/1361-648X/ab5f45

The effect of isomorphic impurities on the elastic conductivity of Dirac structures

Olga S Lebedeva[1,2], Nikolay G Lebedev[1] and Irina A Lyapkosova[3]

[1] Department of Theoretical Physics and Wave Phenomenon, Volgograd State University, Volgograd, Russia
[2] Department of Physics, Volgograd State Agricultural University, Volgograd, Russia
[3] Department of Mechanics, Volgograd State Agricultural University, Volgograd, Russia

E-mail: lebedeva_os@volsu.ru

Received 26 September 2019, revised 27 November 2019
Accepted for publication 5 December 2019
Published 6 January 2020

Abstract

Results of a theoretical study of piezoresistance properties of Dirac structures on example graphene nanoribbons with different types of a conductivity, both ideal and doped with point substitution defects of various concentrations uniformly distributed in the crystal lattice, are presented. Boron and nitrogen atoms are chosen as acceptor and donor impurities respectively. Using the tight-binding method and the Anderson's model, the band structure of the nanoparticles under study is simulated. The longitudinal component of the elastic conductivity tensor is analytically calculated. Its dependence on the relative strain of longitudinal compression and tension, the concentration of impurities and the width of the nanoribbon are studied. The physical substantiation of the results obtained is given.

Keywords: electronic structure, stress–strain state, tensor of elastic conductivity

(Some figures may appear in colour only in the online journal)

1. Introduction

The new carbon-based nanostructures synthesized in 2004, such as graphene and graphene nanoribbons, proved to be materials having a unique set of physic-chemical properties that can be used in a wide range of applied problems [1–4]. The electronic characteristics of graphene vary depending on the nature and concentration of structural defects, atoms and atomic groups adsorbed on its surface [4]. Currently, graphene is one of the main candidates for the elements of nanoelectronics of the future, instead of silicon [4]. Scientists are interested in the unique properties of carbon nanoscale structures, such as high thermal and electrical conductivity, the dependence of electronic characteristics on the presence of attached radicals and impurities of various natures on the surface, extremely high carrier mobility, impurity bandwidth controlled by impurities, high elasticity and good electromechanical characteristics. The main problem of the wide use of graphene in electronics is its small band gap, the opening of which is directed to the main efforts of researchers.

The effect of deformation on the electronic spectrum of crystallite using the example of deformed graphene is described in [5–7]. Under the action of external mechanical actions in the carbon crystallite, stress fields arise that compensate for deformation effects. The induced stress fields can be characterized by the effective vector potential **A**, which acts as a gauge field that changes the electron momentum. The presence of a deformation gauge field **A** in graphene is interpreted in theoretical work [7] as an appearance of a pseudomagnetic field whose induction exceeds 10 T.

The electronic characteristics of carbon nanostructures are quite sensitive to mechanical stress. A change in the energy gap and conductivity of deformed semiconductor carbon nanoparticles leads to the piezoresistance effect, which is quantitatively characterized by piezoresistive constants, such as the elastic-resistance tensor, the piezoresistance tensor, the elastic conductivity tensor and the calibration factor [8]. The piezoresistance effect formed the basis for the development of MEMS [9]—the technology of integration of mechanical elements and sensors on a silicon substrate.

In recent decades, a new scientific direction of condensed matter physics has been formed—straintronics, which uses physical effects in matter due to deformations arising in micro-, nano- and heterostructures under the influence of

external control fields, which lead to a change in the electronic structure, electrical, magnetic, optical and other properties of materials [10]. Similar effects allow implementing a new generation of information and sensor technology devices. For example, in [11] the development of a transistor based on graphene using a deformational change in ballistic conductivity (the effect of piezoconductivity) is announced.

Therefore, despite the 15-year history of the experimental discovery of graphene, its mechanical properties continue to be studied intensively. Bi *et al* have investigated the effect of heterodeformations on moiré bands in twisted two-layer graphene [12]. Transport properties of electrons in graphene under a joint modulation of the magnetic field and the stress barrier as well as a possibility of a pressure control of transport properties of a graphene-based heterostructure are a subject of research in [13, 14] correspondently. The layer ferromagnetism in the framework of the Ising model using Monte Carlo simulations and an induction of a non-collinear magnetism in doped graphene are studed in [15, 16] respectively. One should be noted especially effects associated with quantum phase transitions, namely, breaking of the spin symmetry of singlet state of graphene structures, being caused by deformations [17–19].

Battilomo *et al* [20] have studied Berry curvature dipole in strained graphene and shown that this topological effect arises in 2D Dirac materials even in the complete absence of spin–orbit coupling. Authors of [21] have prognosticated an effect of strain-induced large Faraday rotation in graphene at subtesla external magnetic fields. In [22], the hesteretic behavior of carbon atoms displacements in polycrystalline graphene is predicted based on computer simulation of the discontinuous deformation of its structure. Guinea *et al* [23] have developed continuum models for twisted bilayer graphene and studied an effect of a lattice deformation and variety of hopping parameters. They have shown that the effect causes the band structure and magic angles changes. Authors of [24] have prognosticated the pressure-induced metal–insulator transition in twisted bilayer graphene. The effect of valley engineering by strain in Kekulé-distorted graphene is investigated in [25]. Shear instability in twisted bilayer graphene are represented by authors of [26].

Chernozatonskii *et al* have proposed the method of controlling band gaps in jagged and straight graphene nanoribbons tunable by an external electric field [27, 28], elastic properties of bilayer graphene nanostructures with closed holes [29].

Authors [30] have predicted an anomalous de Haas–van Alphen effect on graphene induced by a mechanical strain. And in [31] *ab initio* calculation results of strain induced armchair graphene nanoribbon demonstrate the possibilities of using deformation properties to manufacture devices for stratronics based on graphene nanoribbons.

This paper presents the results of a theoretical study of the piezoresistive properties of graphene nanoribbons, both ideal and isomorphic impurity. The electronic structure of deformed carbon nanostructures is modelled by introducing a deformation potential that takes into account variations in the interatomic bond lengths and valence angles.

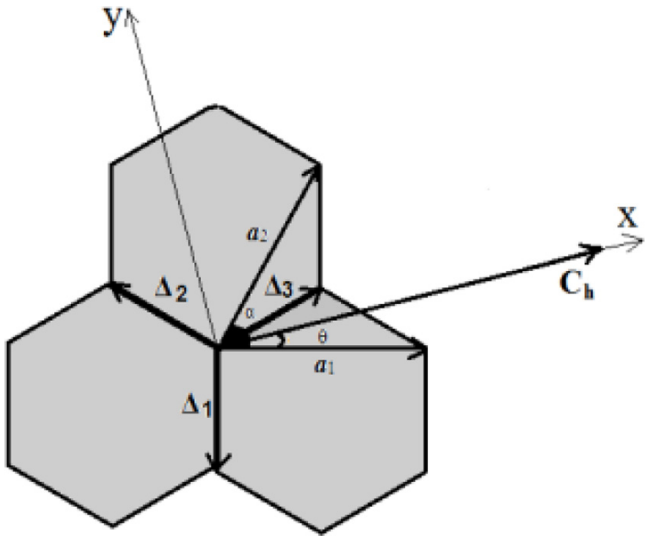

Figure 1. A fragment of the GNR structure, with the selected coordinate system, $\boldsymbol{\Delta_1}$, $\boldsymbol{\Delta_2}$, $\boldsymbol{\Delta_3}$ are the distance vectors between the nearest neighbours, $\boldsymbol{a_1}$, $\boldsymbol{a_2}$ are the translation vectors, α is the angle between the translation vectors, θ is the chiral angle, $\boldsymbol{C_h}$ is the chiral vector.

Previously, the research methodology used in this paper is developed and successfully applied to study the deformation effects in carbon nanotubes (CNTs) [32–34].

2. Model of the electronic structure of deformed nanoribbons

As a geometric model of graphene nanoribbons (GNR), a 2D hexagonal graphene layer is chosen. A fragment of such a graphene crystalline structure is represented in figure 1, which shows the chiral vector $\boldsymbol{C_h} = n\boldsymbol{a_1} + m\boldsymbol{a_2}$, the angle α between the main translation vectors $\boldsymbol{a_1}$ and $\boldsymbol{a_2}$, and the vectors of interatomic distances $\boldsymbol{\Delta}_i$. The coordinate system is chosen in such a way that the width of the ribbon is measured along the *OX* axis using the chiral vector $\boldsymbol{C_h}$, and the *OY* axis is directed along the length of GNR. The angle $\theta = \angle(\boldsymbol{C_h}, \boldsymbol{a_1})$ is measured from the translation vector $\boldsymbol{a_1}$, lies in the range $0 \div 30°$ and is called the chiral angle [4].

A mathematical model of the electronic structure of non-deformed GNRs is constructed based on its geometric structure and the band structure of the graphene layer [4]. The general form of the band structure of graphene nanoribbons in the framework of the tight-binding method in the approximations of Hückel and nearest neighbours can be represented in the form [4]:

$$\varepsilon(\boldsymbol{k}) = \pm\gamma_0 \left\{3 + 2\cos\left(\boldsymbol{k}\boldsymbol{a}_1\right) + 2\cos\left(\boldsymbol{k}\boldsymbol{a}_2\right) + 2\cos\left(\boldsymbol{k}\left(\boldsymbol{a}_1 - \boldsymbol{a}_2\right)\right)\right\}^{1/2} = \\ = \pm\gamma_0 \left\{1 + 4\cos\left(\frac{\boldsymbol{k}(\boldsymbol{a}_1+\boldsymbol{a}_2)}{2}\right)\cos\left(\frac{\boldsymbol{k}(\boldsymbol{a}_1-\boldsymbol{a}_2)}{2}\right) + 4\cos^2\left(\frac{\boldsymbol{k}(\boldsymbol{a}_1-\boldsymbol{a}_2)}{2}\right)\right\}^{1/2}, \quad (1)$$

where γ_0 is the hopping integral, the matrix element of the electron transition between adjacent carbon atoms, $\mathbf{k}$ is the wave vector, one of the components of which is quantized along the width of GNR. The Fermi level in the dispersion law (1) is taken as 0 eV.

The quantization condition for the wave vector **k** along the direction of the chiral vector $\mathbf{C_h}$ can be written as follows [4]:

$$\mathbf{k} \cdot \boldsymbol{C}_\mathbf{h} = 2\pi q, \text{where } q = 1, 2, \ldots \tag{2}$$

It is advisable to choose k_x and k_y components of the wave vector so that they are aligned with the chiral vector $\boldsymbol{C}_\mathrm{h}$ and the GNR length, respectively, i.e. $\mathbf{k}_x \uparrow\uparrow \mathbf{C}_\mathrm{h}$ and $\mathbf{k}_y \perp \boldsymbol{C}_\mathbf{h}$. The module of the chiral vector of non-deformed GNR can be represented, based on its definition, in the following known form [4]:

$$|\boldsymbol{C}_{h0}| = \sqrt{n \cdot \boldsymbol{a}_1^2 + m \cdot \boldsymbol{a}_2^2 + 2nm\boldsymbol{a}_1\boldsymbol{a}_2} = a\sqrt{n^2 + m^2 + nm}. \tag{3}$$

Using (3) and conditions (2), we can obtain an explicit expression for quantization of the transverse component of the wave vector:

$$k_x a = \frac{2\pi q}{\sqrt{n^2 + m^2 + nm}}, \quad q = 1, 2, ..., \left[\sqrt{n^2 + m^2 + nm}\right]. \tag{4}$$

The scalar products of the wave vector by the half-sum and half-difference of the vectors of the main translations included in arguments of the trigonometric functions in the expression for the band structure (1), based on the geometric transformations corresponding to figure 1, can be written as follows:

$$\begin{aligned} \frac{\boldsymbol{k}(\boldsymbol{a}_1+\boldsymbol{a}_2)}{2} &= \left(\frac{1}{\sqrt{n^2+m^2+nm}} \cdot \left(\frac{3\pi q(n+m)}{2\sqrt{n^2+m^2+nm}} + \frac{\sqrt{3}k_y a(n-m)}{4}\right)\right), \\ \frac{\boldsymbol{k}(\boldsymbol{a}_1-\boldsymbol{a}_2)}{2} &= \left(\frac{1}{\sqrt{n^2+m^2+nm}} \cdot \left(\frac{\pi q(n-m)}{2\sqrt{n^2+m^2+nm}} - \frac{\sqrt{3}k_y a(n+m)}{4}\right)\right). \end{aligned} \tag{5}$$

As a result, expression (1) and relations (5) completely determine the energy spectrum of electrons of non-deformed GNR. According to the GNR electronic structure theory [4], a set of dispersion curves of the electronic spectrum, numbered by the integer q, is formed by crossing the 2D energy surface of graphene with parallel planes corresponding to the continuous component of the wave vector. It position relative to the Brillouin's zone is given by the discrete value k_x-components of the wave vector according to the quantization condition (2).

The deformed state of a crystallite is generally characterized by a distortion tensor $u_{\alpha\beta} = \partial_\beta(\mathbf{r}' - \mathbf{r})_\alpha$, ($\alpha$, $\beta = x$, y, z), where **r** и **r**′—radius vectors of the initial and final position of a crystallite point [37]. The diagonal elements of the tensor characterize the relative elongation of the sample along the corresponding direction; the off-diagonal elements specify the angle of rotation of the linear element during deformation.

Based on the definition of the distortion tensor, the obtaining of the energy spectrum of deformed GNRs is based on a modification of the scalar products that appear in the arguments of trigonometric functions in the expression of the electronic spectrum (1). The change in the GNR unit cell under an action of a tensile deformation is shown in figure 2. The Figure demonstrates the model idea of that, due to deformation, not only the interatomic bond lengths $\Delta_i = R_0(1 + \delta)$, where $\delta = \Delta R/R_0$, are changed by its elongation, but the angle between the translation vectors $\alpha = \alpha_0 + \Delta\alpha$ ($\alpha_0 = \pi/3$ is the angle between the translation vectors in the non-deformed lattice) also. Therefore, projections of the translation vectors

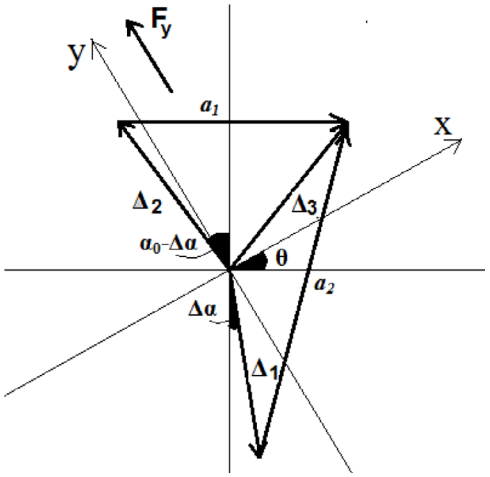

Figure 2. Positions of interatomic vectors $\boldsymbol{\Delta_1}$, $\boldsymbol{\Delta_2}$, $\boldsymbol{\Delta_3}$ after deformation of tension (compression) taking into account its rotation through the angle $\Delta\alpha$.

$\boldsymbol{a_1}$ and $\boldsymbol{a_2}$ on the *OX* and *OY* axes of the selected coordinate system are changed item.

An expression for the band structure of deformed GNRs can be obtained from geometric transformations (figure 2). As a result, the electronic spectrum of such nanoribbons take the form:

$$\begin{aligned} \varepsilon(\mathbf{k}) = \pm\gamma(1 + 4\cos[\pi nA_1 + B_1]\cos[\pi nA_2 - B_2] \\ +4\cos^2[\pi nA_2 - B_2])^{1/2}, \end{aligned} \tag{6}$$

where the following notation is introduced for the general case:

$$\begin{aligned} A_1 &= \tfrac{F\cos\alpha + G\sin\alpha}{A\cos\alpha + B\sin\alpha}, \quad A_2 = \tfrac{-E\cos\alpha}{A\cos\alpha + B\sin\alpha}, \\ B_1 &= k_y R_0(1+\delta)(-G\cos\alpha + F\sin\alpha), \\ B_2 &= k_y R_0(1+\delta)E\sin\alpha, \end{aligned} \tag{7}$$

$$\begin{aligned} A &= n\sin\theta\cos(2\alpha_0) + m\cos\theta\cos(\alpha_0/2), \\ B &= \sin\theta[n\sin(2\alpha_0) + m\cos(\alpha_0/2)], \\ E &= \sin\theta\sin(\alpha_0/2) + \cos\theta\cos(\alpha_0/2), \\ F &= \sin\theta\cos(2\alpha_0) + \cos\theta\cos(\alpha_0/2), \\ G &= \sin\theta[\sin(2\alpha_0) + \cos(\alpha_0/2)]. \end{aligned} \tag{8}$$

The change in the transverse sizes (width) of the GNR as a result of deformation is taken into account by modifying the modulus of the chiral vector $\boldsymbol{C}_\mathbf{h}$, which, based on the determination of the Poisson's ratio and direct proportionality of the main geometric sizes of the nanoribbons to the lattice parameters, can be calculated using the following formula:

$$C_h = (1\nu \cdot \delta)C_{h0}, \tag{9}$$

where ν is the Poisson's ratio, the value of which varies within the limits of $\nu = 0.19 \div 0.27$.

The relation (9) and the selected geometric model of deformed GNR allow us to determine the angle α between the translation vectors in the deformed hexagonal lattice, which is included in the expressions for the coefficients (7) and (8) of the spectrum of nanoribbons (6):

$$\sin\alpha = \frac{BC + A\sqrt{B^2 - C^2 + A^2}}{A^2 + B^2}, \tag{10}$$

where

$$C = \frac{1-\nu\delta}{1+\delta}\left[\sin\theta\left(n\cos\alpha_0 + m\cos^2\left(\frac{\alpha_0}{2}\right)\right) + \frac{m}{2}\cos\theta\sin\alpha_0\right],$$

and the coefficients A and B are expressed by formula (8).

The procedure for calculating the dependence of the hopping integral $\gamma(\delta)$ on the strain using carbon nanotubes as an example is clearly described in [32–34].

For theoretical calculations, the following values of the strain (compression) $\delta = \pm 0.035,\ \pm 0.069,\ \pm 0.104,\ 0.25$, corresponding to the interatomic bond lengths $R = 1.49, 1.54, 1.59, 1.8$ Å in the case of tension and $R = 1.39, 1.34, 1.29$ Å in the case of compression, are used in the work.

Principal qualitative differences between the obtained band structures of semiconductor arm-chair type GNRs compared with the energy spectrum of non-deformed nanoribbons are not observed. A quantitative analysis shows a narrowing of the conduction band (CB), valence band (VB) and the band gap, which leads to an increase in the density of electronic states in the case of compression and, conversely, broadening of the CB, VB and band gap (decrease in the density of states) under tensile strain. A similar effect was also observed in the case of deformation of achiral (arm-chair and zig-zag types) carbon nanotubes studied in [32–36].

In the case of conducting arm-chair and zig-zag GNRs, longitudinal tension (compression) also changes its band structure in the manner described above and does not fundamentally distinguish them from arm-chair nanoribbons. With one exception, the energy gap in such GNR is absent and does not open at small deformations. The opening of the gap by deformation of the structure can be observed in mixed GNRs, as in the case of chiral CNTs [36], in which Mott transitions such as 'conductor–semiconductor' and 'semiconductor–conductor' become possible due to axial tensile (compression) strains.

3. Model of the electronic structure of impurity graphene nanoribbons

The presence of isomorphic donor and acceptor impurities (point substitution defects) in the crystalline structure of GNRs can significantly affect its band structure and piezoconductivity, as shown by the example of nanotubes in [34–36]. To describe the electronic structure of impurity nanoribbons, the Anderson's periodic model is used [38]. This model, as a rule, is used to describe the electronic states of a crystal with low concentrations of defects, the interaction of which is small compared with the electron energy of an unperturbed crystal. It consists of a separate consideration of two groups of electrons: collectivized and localized, the interaction between which is carried out through the potential of hybridization. The electron-phonon interaction in the model is not taken into account. The π-electron approximation for GNR is used in the framework of the model, and collectivized electrons are considered in the periodic crystal approximation. The electronic GNR spectrum in the framework of the Anderson's model has the following form [38]:

$$E(\mathbf{k}) = \frac{1}{2}\left[\varepsilon_l + \varepsilon(\mathbf{k}) \pm \sqrt{(\varepsilon_l - \varepsilon(\mathbf{k}))^2 + 36|V_{\mathrm{CD}}|^2 \cdot x}\right], \tag{11}$$

where $\varepsilon(\mathbf{k})$ is the band structure of an ideal nanoribbon expressed by formula (6), ε_l is the electron energy at the defect, $x = N_d/N$ is the concentration of impurities, N is the number of unit cells in the crystal, N_d is the number of point defects, V_{CD} is the hybridization energy of the crystal electrons and electron point defect.

Boron and nitrogen atoms, respectively, are chosen as acceptor and donor impurities. The electron energy at the defect (nitrogen atom) is calculated as the difference between the ionization potentials (electron work function) of the nitrogen and carbon atoms:

$$\varepsilon_l = I_C - I_N = 11.25\,\mathrm{eV} - 14.53\,\mathrm{eV} = -3.28\,\mathrm{eV}.$$

The V_{CD} hybridization potential parameter is calculated using the resonance integral formula in the framework of the quantum chemical semi-empirical MNDO method [39]:

$$V_{lj} = \left\langle \psi_l \left| -\frac{\hbar^2}{2m}\nabla^2 + V_l + V_j \right| \psi_j \right\rangle \approx \frac{1}{2}(\beta_{\mathrm{C}} + \beta_{\mathrm{D}})S_{\mathrm{CD}}, \tag{12}$$

$$\begin{aligned} S_{\mathrm{CD}} &\equiv S_{\mathrm{pp}} = \int \Psi_{2p_z}(\boldsymbol{R}_{\mathrm{D}} - \mathbf{r})\Psi_{2p_z}(\mathbf{r})\mathrm{d}\mathbf{r}, \\ \Psi_{p_z}(\mathbf{r}) &= \tfrac{1}{4\sqrt{2\pi}}\left(\tfrac{Z}{a_0}\right)^{\frac{3}{2}}\boldsymbol{\rho}\exp(-\boldsymbol{\rho}/2)\cos\phi, \end{aligned} \tag{13}$$

where V_l and V_j are the interaction potentials of the electron with the lth and jth lattice sites, S_{CD} is the overlap integral of $2p_z$ atomic orbitals Ψ_j and Ψ_l localized on the jth carbon atom and the lth defect atom, respectively, β_{C} and β_{D} are the resonance parameters of the MNDO metod for a carbon atom and a defect atom, respectively, $\boldsymbol{\rho} = Z^*\mathbf{r}/a_0$, $\mathbf{r}(r, \phi, \varphi)$ is the dimensionless electron radius vector, a_0 is the Bohr radius, Z is the atomic number. In accordance with the MNDO method, atomic wave functions are selected in the form of Slater orbits with an effective charge number Z^*. The value of the resonance constants β_{D} of the MNDO method is $\beta_{\mathrm{B}} = -8.25\,\mathrm{eV}$ for the boron atom and $\beta_{\mathrm{N}} = -20.4\,\mathrm{eV}$ for the nitrogen atom. After numerical integration by the Simpson method [40], the potentials of V_{CD} electrons at the impurity atom are $V_{\mathrm{CB}} = -1.7\,\mathrm{eV}$ and $V_{\mathrm{CN}} = -1.8\,\mathrm{eV}$ for boron and nitrogen, respectively.

The final expression for the band structure of deformed impurity GNRs is obtained by substituting expression (6) into formula (11). As in the case of CNTs, the introduction of a point acceptor substitution defect (boron atom) into the crystallite structure promotes the appearance of an impurity band and an energy gap at the Fermi level in the spectrum of conducting and semiconductor nanoribbons. With an increase in the relative compressive (tensile) deformation, the band gap in the impurity band sequential broadens (narrowing), and the density of states in the CB decreases (increases). This is due to a change of the hopping integral (electron energy) and hybridization potential, which leads to an increase (weakening) of the interaction of impurities with the crystallite, respectively.

A consequence of the latter is an increase (decrease) in the splitting of the impurity level.

4. Elastoconductivity of graphene nanoribbons

The piezoresistive effect is characterized by tensors of elastoconductivity, elastoresistance or the so-called gauge factor [8]. The components of the elastoconductivity tensor can be calculated theoretically, and the elastoresistance tensor can be measured experimentally. According to the definition, the 4th rank tensor of elastroconductivity $M_{\alpha\beta\gamma\delta}$ can be represented by the following formula [8]:

$$\begin{gathered}\frac{\Delta\sigma_{\alpha\beta}}{\langle\sigma\rangle} = M_{\alpha\beta\gamma\delta}\cdot\varepsilon_{\gamma\delta},\\ \langle\sigma\rangle = \tfrac{1}{2}Sp\left[\widehat{\sigma}\right] = \tfrac{\sigma_{xx}+\sigma_{yy}}{2},\\ M_{\alpha\beta\gamma\delta} = M_{\beta\alpha\gamma\delta} = M_{\beta\alpha\delta\gamma} = M_{\alpha\beta\delta\gamma},\end{gathered} \tag{14}$$

where $\sigma_{\alpha\beta}$ is the 2nd rank tensor of the conductivity; α, β, γ, $\delta = x, y$.

The calculation of piezoresistive constants (the longitudinal component of the elastoconductivity tensor) GNR is carried out according to the method described in detail in [32–34]. Based on the definition of the elastic conductivity tensor [8], its longitudinal component for 1D structures can be expressed by the following formula:

$$M = \frac{\Delta\sigma}{\sigma_0}\frac{1}{\delta}, \tag{15}$$

where $M = M_{xxxx}$, M_{yyyy} is the longitudinal component of the tensor of the 4th rank of elastic conductivity for armchair and zigzag GNR respectively, $\Delta\sigma = \sigma - \sigma_0$ is the change in the longitudinal component of the conductivity tensor due to crystallite deformation, σ and σ_0 are the longitudinal components σ_{xx} or σ_{yy} of the tensor of the 2nd rank of the conductivity of the deformed and non-deformed armchair and zig-zag GNR, respectively.

The longitudinal component of the non-phonon conductivity tensor of the GNT is calculated in the framework of the Kubo–Greenwood theory using the Green's function method and the model tight-binding Hamiltonian [41]. The final expression for the GNR longitudinal conductivity used in the calculations of the constant M has the following form [33]:

$$\sigma = 2\frac{i\pi e^2}{k_B TV}\sum_{\mathbf{k},\alpha}\sum_{\mathbf{q},\beta} v(\mathbf{k})v(\mathbf{q})\,\langle n_{\mathbf{k}\alpha}\rangle\,[\langle n_{\mathbf{q}\beta}\rangle + \delta_{\mathbf{kq}}\delta_{\beta\alpha}\,(1-\langle n_{\mathbf{k}\alpha}\rangle)], \tag{16}$$

where V is the crystallite volume, k_B is the Boltzmann constant, T is the absolute temperature, e is the elementary charge, $\mathbf{k}$, $\mathbf{q}$ are two-component wave vectors within the Brillouin's zone (BZ), α, β are the spin indices, v is the longitudinal component of the electron velocity vector in the BZ, which determined in a standard way using the electronic spectrum $E(\mathbf{k})$:

$$\mathbf{v}(\mathbf{k}) = \frac{1}{\hbar}\frac{\partial E\,(\mathbf{k})}{\partial\mathbf{k}}. \tag{17}$$

$\langle n_{\mathbf{k}\alpha}\rangle$ is the average number of particles in a quantum state with wave vector $\mathbf{k}$ and spin α, expressed by the Fermi–Dirac distribution function.

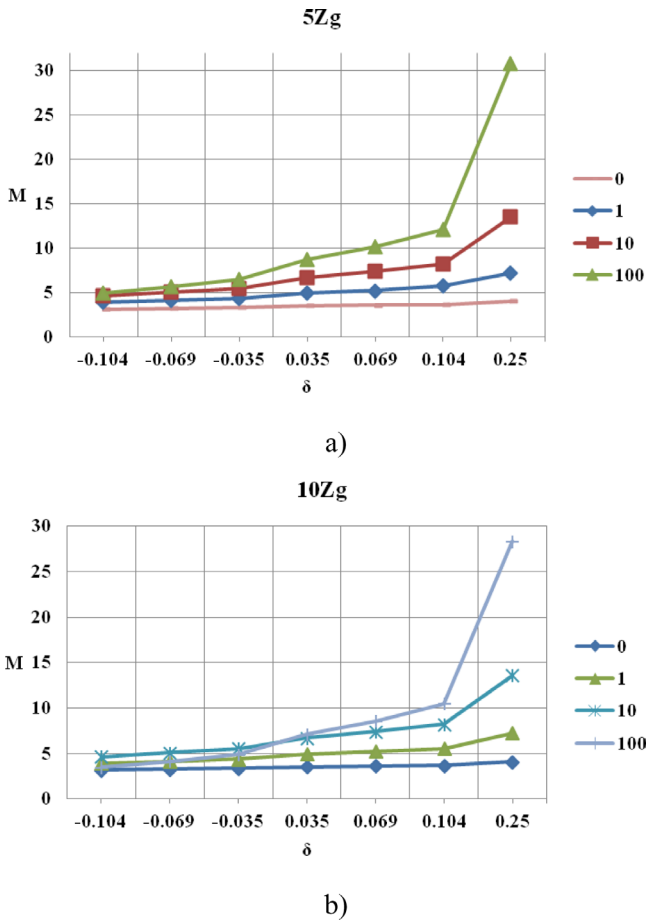

Figure 3. The longitudinal component M of the elastic conductivity tensor of zig-zag GNRs with a width of 5 (a) and 10 (b) UCs as a function of the strain δ with various concentration of acceptor defects (boron atoms) $N_d = 0, 1, 10, 100$. On all curves, the point $\delta = 0$ is not defined.

Since numerous studies of the transport properties of graphene nanoribbons indicate the ballistic (non-phonon) nature of electronic conductivity, the use of a tight-binding model that does not take into account the electron-phonon interaction is justified and appropriate.

Dependences of the component M of the elastic conductivity tensor on the relative deformation δ ($= -0.104$, -0.069, -0.035, 0.035, 0.069, 0.104, 0.25) for arm-chair (nArm, where $n = 9, 10, 50, 100$ unit cells along a width) and zig-zag (mZg, where $m = 5, 10$) GNRs of different widths, and the type of conductivity are shown in figures 3 and 4. Numerical results are obtained at a temperature of $T = 300$ K. For a clear image of the tendency for the constant M to change, the calculated points are connected by solid lines. It should be understood that the point $\delta = 0$ is not defined.

As follows from the figures, the longitudinal component M of the conductive arm-chair (9Arm) and zig-zag (5Zg, 10Zg) GNRs is positive and its behaviour completely correlates with the changes in the band structure described above. The general pattern for the considered conducting nanoribbons is a monotonic increase (decrease) of the value of M with an increase of the strain δ. A similar behaviour is observed in conducting achiral CNTs [32, 33]. Despite the increase in the width of

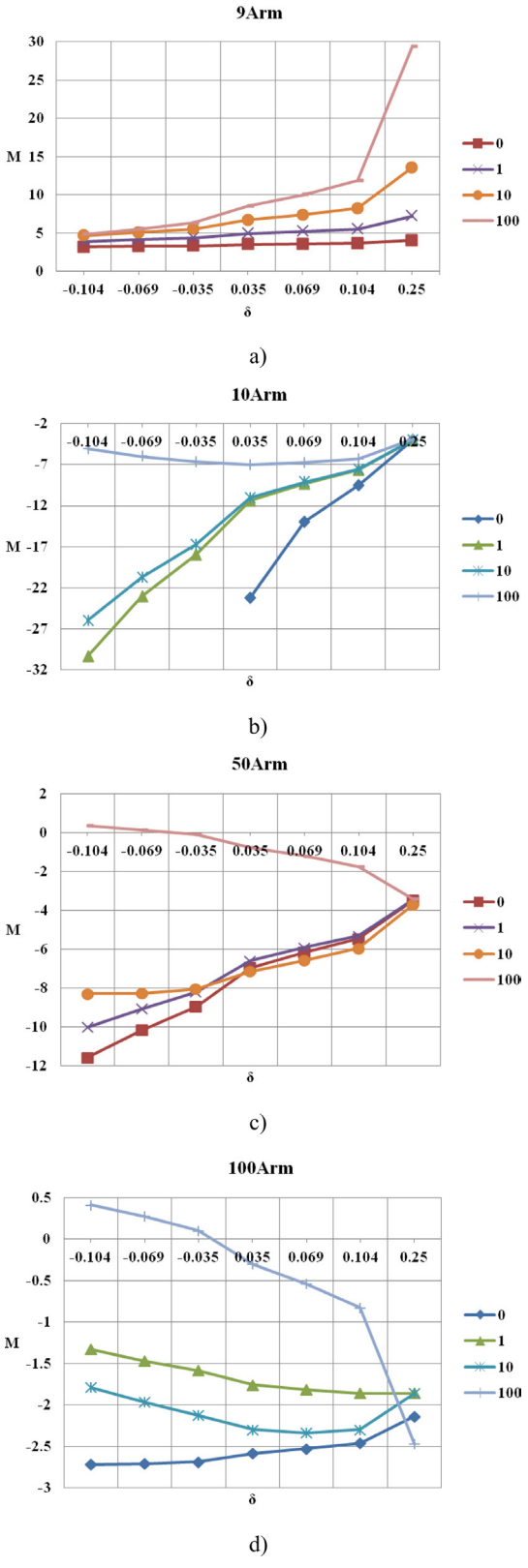

Figure 4. The longitudinal component M of the elastic conductance tensor of arm-chair GNRs with a width of 9 (a), 10 (b), 50 (c) and 100 (d) UCs as a function of the strain δ with various concentration of acceptor defects (boron atoms) $N_d = 0, 1, 10, 100$. On all curves, the point $\delta = 0$ is not defined.

the conduction band and a decrease in the density of states at the Fermi level with increasing δ, the conductivity increases, that leads to a monotonic growth of the component M. This effect is associated with the fact that an increasing number of charge carriers with ever higher energies give contribution to the conductivity of the crystallite. Thermal fluctuations lead to the filling of the GNR conduction band by electrons according to the Fermi–Dirac distribution function. A modification of the electronic spectrum leads to a change of the conductivity, taking into account all possible filled electronic states, and, consequently, to an increase in the component M with a growth of δ.

In the case of semiconductor arm-chair (10Arm, 50Arm, 100Arm) GNR, the longitudinal component M is negative, but, as in the case of conducting nanoribbons, it monotonically increases with a growth of δ. The negative value is due to a decrease of the conductivity with increasing the strain. This effect is also a consequence of the behaviour of the band structure of deformed semiconductor GNRs, in which the energy gap broadens and, therefore, the number of occupied states in the CB decreases. A similar behaviour of the constant M is also observed in semiconductor achiral CNTs [32, 33].

The longitudinal component M of semiconductor arm-chair (10Arm, 50Arm, 100Arm) GNR, as opposed to conductance these, increases with growing a width of the nanoribbon. And the smaller the deformation, then the M value changes more. This behaviour is determined by a decrease in the band gap with a decrease in the strain δ and an increase in the nanoribbon width.

5. The effect of isomorphic impurities on the piezoelectric conductivity of graphene nanoribbons

The piezoresistance constants M of the impurity arm-chair and zig-zag GNRs are calculated based on formula (15) with the term (16), which includes the expression for its band structure (11). The presence of donor and acceptor substitution defects in the crystal lattice modifies the GNR energy spectrum in accordance with the dispersion relation (11). Calculation data for the longitudinal component of the elastic conductivity tensor of arm-chair and zig-zag GNRs with acceptor and donor impurities (boron and nitrogen atoms respectively) added to the crystal lattice as functions of the tensile (compression) strain δ are shown in figures 3–6.

As follows from the analysis of the calculation results, small additions of acceptor impurities (boron atoms) $N_d = 1$, 10, 100 per $N = 100\,000$ unit cells (UC) in crystallite of conducting arm-chair (9Arm) and zig-zag (5Zg, 10Zg) GNRs affect by the component M, which increases at each strain value δ with an increase in the concentration of acceptor impurities in comparison with ideal structures (figures 3 and 4). Boron atoms embedded in the atomic lattice of the nanoribbon create a band of impurity states near the Fermi level and a small energy gap at the level itself, which increases with growing of impurity concentrations. But at the same time, the density of states increases near the Fermi level. A consequence of the described change in the band structure is an increase of the conductivity of metallic GNRs and the piezoresistance constant M.

It should be noted that the M value of conducting nanoribbons, both ideal and with impurity, is practically independent of their width. That is, the band structure of such nanoribbons near the Fermi level is identical.

The behaviour of the longitudinal component M of impurity semiconductor arm-chair (10Arm, 50Arm) GNRs is similar to the behaviour of the ideal nanoribbon constant. In most cases ($N_d = 1$, 10), a monotonic growth with increasing strain δ is observed.

For 100Arm GNR, a monotonic decrease in case $N_d = 1$ and a monotonic decrease to the extreme point $\delta = 0.069$, after which a monotonic growth begins, with $N_d = 10$ are observed. For these nanoribbons, competing effects begin to appear. The first effect is the inversely proportional dependence of the band gap E_g on the nanoribbon width H ($E_g \sim 1/H$) [42–44]. The second effect is associated with an increase in the energy band with growing the strain. In addition, the third effect appears when the Brillouin's zone is deformed. At the same time, the transverse sizes of the ribbon and, therefore, the quantization step of the transverse component of the wave vector are reduced. As a result, parallel planes cutting a 2D energy surface of graphene are closer to the Dirac points. This, in turn, leads to a decrease in the band gap and an increase in the specific conductivity of the 1D crystallite.

The question about that, at what GNR width the trend in the functional dependence of $M(\delta)$ is changing, remains open at the moment.

The case of the defect concentration $N_d = 100$ requires a separate consideration. For 10Arm GNR, the $M(\delta)$ function has a minimum at the point $\delta = 0.035$. One should be noted that this point is minimal in the considered discrete strain range. Further growth of the constant $M(\delta)$ is caused by the following. The tensile strain increases the band gap, but simultaneously narrows the conduction and impurity bands. Because of the latter, the density of states near the Fermi level increases, which ultimately leads to an increase in conductivity at a finite temperature.

For wide nanoribbons (50Arm, 100Arm), the component M is decreasing over the entire range of strain δ. In the negative region ($\delta < 0$), it takes a positive value, as well as for conducting GNR. Most likely, the effects of a decrease of E_g because of the structure deformation and an increase in the density of states due to the narrowing of the impurity band are predominated here. In the positive region ($\delta > 0$), the effects of broadening of the band gap E_g and the energy gap of the impurity band become dominant. This leads to a decrease in conductivity, causing a decrease in the function $M(\delta)$.

Weak oscillations, which is observed on the $N_d = 100$ curves, are most likely associated with the unevenness of the used scale δ (figures 4(c) and (d)).

In the case of donor impurities (nitrogen atoms), an insignificant change in the piezoresistance constant of conducting zig-zag (5Zg, 10Zg) (figure 5) and arm-chair (9Arm) (figure 6(a)) GNRs is observed for each given strain δ for small concentrations $N_d = 1$, 10, 100. Therefore, the function $M(\delta)$ for such GNRs is similar to the function for nanoribbons both ideal and with acceptor impurities (figures 3 and 4). Only high concentrations of defects ($N_d = 1000$, 10 000) lead to a significant change in the constant M for large deformations (figure 5).

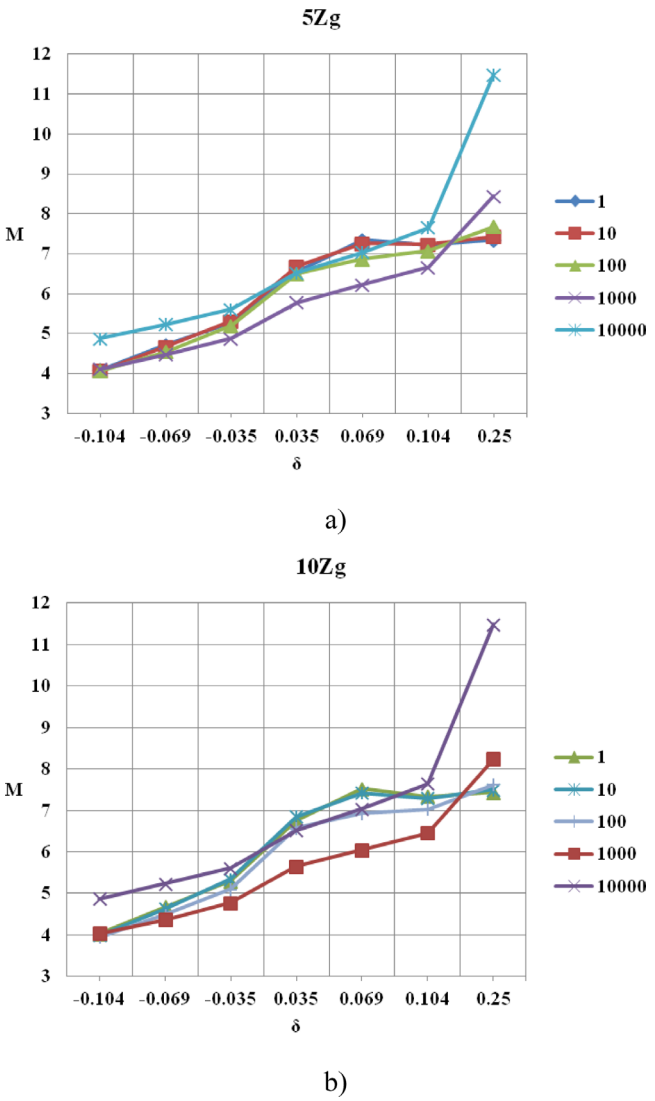

Figure 5. The longitudinal component M of the elastic conductivity tensor of zig-zag GNRs with a width of 5 (a) and 10 (b) UCs as a function of the strain δ with various concentration of donor defects (nitrogen atoms) $N_d = 1$, 10, 100, 1000, 10 000 and the relative strain δ. On all curves, the point $\delta = 0$ is not defined.

As mentioned above, the donor defect levels create a band of impurity states in the valence band, practically without changing the density of states at the Fermi level. Therefore, the behavior of the function $M(\delta)$ is characteristic of both conductive nanoribbons (figures 3 and 4(a)).

The longitudinal component of the elastic conductivity tensor M of semiconductor arm-chair (10Arm, 50Arm, 100Arm) GNR takes a positive value and generally monotonically decreases with increasing strain value until $\delta = 0.069$, than it grows tothe limited point $\delta = 0.25$ (figures 6(b)–(d)). This is due to the fact that the deformation of the nanoribbon structure increases the band gap, as mentioned above. However, donor nitrogen atoms form a zone of impurity states near the defect level, which is localized in the valence band and leads to broadening of the VB and an increase in the density of states in the vicinity of the Fermi level. At a finite temperature

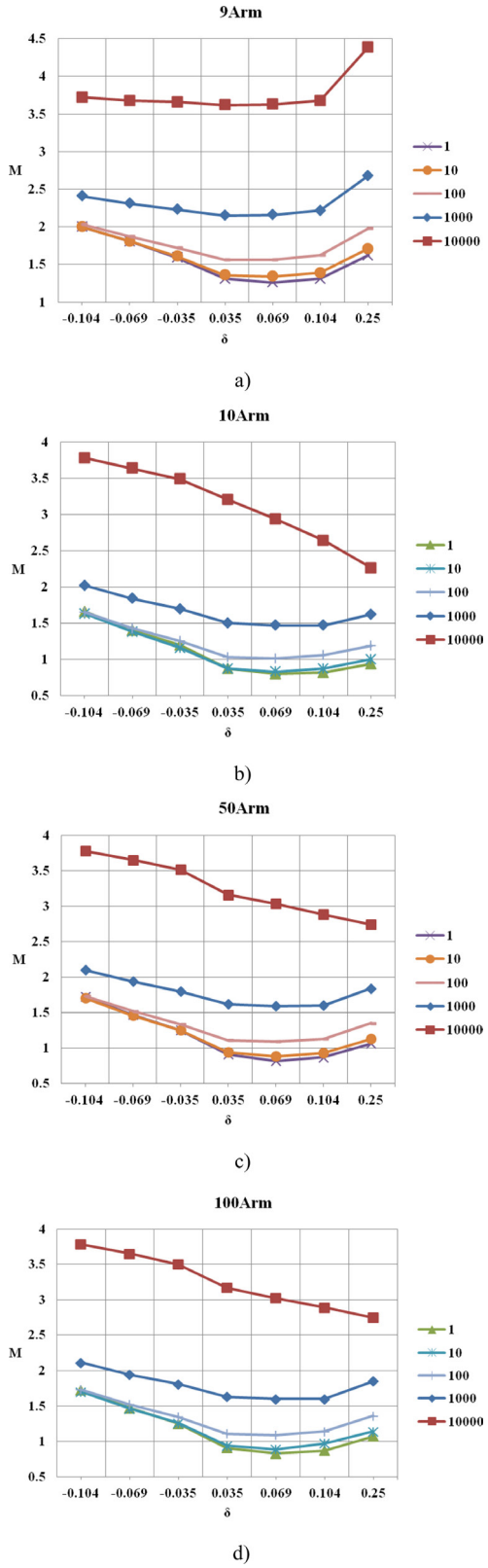

Figure 6. The longitudinal component M of the elastic conductivity tensor of arm-chair GNRs with a width of 5 (a), 10 (b), 50 (c) and 100 (d) UCs as a function of the strain δ with various concentration of donor defects (nitrogen atoms) $N_d = 1$, 10, 100, 1000, 10 000. On all curves, the point $\delta = 0$ is not defined.

donor impurities increase the number of charge carriers in the CB due to thermal fluctuations taken into account using the Fermi–Dirac distribution. The competition of the described effects ultimately leads to an increase in GNL conductivity. Therefore, despite the semiconductor nature of the band structure, the constant M of 10Arm, 50Arm and 100Arm GNR with donor impurities is positive and decreasing.

In addition, in the case of large deformations ($\delta > 0.069$), another effect begins to play a significant role; this is associated with the narrowing of the Brillouin's zone. At the same time, the transverse dimensions of the ribbon and, therefore, the quantization step of the transverse component of the wave vector are reduced. As a result, parallel planes cutting a 2D energy surface of graphene are closer to the Dirac points. This, in turn, leads to a decrease in the band gap and an increase in the specific conductivity of the 1D crystallite. This effect is reflected in the behavior of the curve $M(\delta)$ at large δ; the $M(\delta)$ begins to increase monotonically.

It should be noted that it cannot be stated with accuracy that the strain $\delta = 0.069$ is an extreme of the function $M(\delta)$. To determine the true minimum of this function, further numerical studies are needed.

As follows from the results presented in figure 6, only a high concentration of donor defects (untill $N_d = 10\,000$, $x = 0.1$) can significantly increase the piezoresistance constant M of semiconductor GNR. In addition, these curves do not show an evidently extreme in the considered range of δ and decreases monotonically. In this regard, the behaviour of the curves is similar to the corresponding functions $M(\delta)$ for the case of acceptor defects, only the component M remains positive. Apparently, the dominant contribution in these dependences is the effect of the E_g increase with a strain growth, which decreases the specific conductivity of the crystallite. This is reflected in the decline in function $M(\delta)$.

The question also remains open at what value of the concentration of donor defects the curve $M(\delta)$ changes its tendency.

6. Conclusion

A theoretical study of the piezoresistive properties of impurity graphene nanoribbons in the framework of the tight-binding method revealed a number of features of the behaviour of the longitudinal component of the elastic conductivity tensor discussed above. A quantitative study of the dependences of the constant M on the strain value and the type and concentration of isomorphic impurities allows us to obtain a more complete picture of the change in the conductivity of graphene nanoribbons due to the strain of axial tension (compression).

The results can also be adapted for electromechanical nanosensor developments, which are based on the effect of piezoelectric resistance, and graphene nanoribbons are the main structural element. The operating characteristics of the sensors can be purposefully changed by varying the concentration of donor and acceptor substitution defects.

It is assumed that the studied piezoresistive properties of graphene nanoribbons are common to the whole family of Dirac structures, including silicene, germanene, stanene and so on nanoribbons.

Acknowledgments

The reported research was funded by Russian Foundation for Basic Research and the Government of Volgograd Region, Grant № 18-42-343004.

ORCID iDs

Olga S Lebedeva https://orcid.org/0000-0002-3502-9570
Nikolay G Lebedev https://orcid.org/0000-0002-4400-8982

References

[1] Morozov S V, Novoselov K S and Geim A K 2008 *Phys. Usp.* **51** 744–8
[2] Lozovik Yu E, Merkulova S P and Sokolik A A 2008 *Phys. Usp.* **51** 727–44
[3] Chernozatonskii L A, Sorokin P B and Artukh A A 2014 *Russ. Chem. Rev.* **83** 251–79
[4] Aoki H and Dresselhaus M S 2014 *Physics of Graphene* (Switzerland: Springer)
[5] Sasaki K, Kawazoe Y and Saito R 2005 *Prog. Theor. Phys.* **113** 463
[6] Maenes J L 2007 *Phys. Rev.* B **76** 045430
[7] Suzuura H and Ando T 2002 *Phys. Rev.* B **65** 235412
[8] Bir G L and Pikus G E 1974 *Symmetry and Strain-Induced Effects in Semiconductors* (New York: Wiley) 484
[9] Vostrikov M V 2007 *Naukoemkie Tehnologii. MGTU imeni N.Je. Baumana [High Technology. MSTU Named After N.E. Bauman]* (Moscow: Bauman Moscow Technical State University) pp 223–8 [in Russian]
[10] Bukharaev A A, Zvezdin A K, Pyatakov A P and Fetisov Yu K 2018 *Phys. Usp.* **61** 1175
[11] McRae A C, Wei G and Champagne A R 2019 *Phys. Rev. Appl.* **11** 054019
[12] Bi Zh, Yuan N F Q and Fu L 2019 *Phys. Rev.* B **100** 035448
[13] Lu J-D, Liu H-Y and Peng S-J 2019 *J. Magn. Magn. Mater.* **489** 165478
[14] Chantngarma P and Soodchomshomb B 2019 *J. Magn. Magn. Mater.* **473** 291–5
[15] Ivashko V, Angelsky O and Maksimyak P 2019 *J. Magn. Magn. Mater.* **492** 165617
[16] Liang J T, Yan X H, Zhang Y, Guo Y D and Xiao Y 2019 *J. Magn. Magn. Mater.* **480** 101–7
[17] Akinwande D *et al* 2017 *Extreme Mech. Lett.* **13** 42
[18] Sheka E 2017 *Spin Chemical Physics of Graphene* (Singapore: Pan Stanford Publishing) 493
[19] Sheka E F, Popova N A and Popova V A 2018 *Phys. Usp.* **61** 645–91
[20] Battilomo R, Scopigno N and Ortix C 2019 *Phys. Rev. Lett.* **123** 196403
[21] Slipchenko T M, Schiefele J, Guinea F and Martín-Moreno L 2019 *Phys. Rev. Res.* **1** 033049
[22] D'Ambrosio F, Juričić V and Barkema G T 2019 *Phys. Rev.* B **100** 161402
[23] Guinea F and Walet N R 2019 *Phys. Rev.* B **99** 205134
[24] Padhi B and Phillips Ph W 2019 *Phys. Rev.* B **99** 205141
[25] Andrade E, Carrillo-Bastos R and Naumis G G 2019 *Phys. Rev.* B **99** 035411
[26] Lin X, Liu D and Tománek D 2018 *Phys. Rev.* B **98** 195432
[27] Saroka V A, Batrakov K G, Demin V A and Chernozatonskii L A 2015 *J. Phys.: Condens. Matter* **27** 145305
[28] Chernozatonskii L A, Demin V A and Lambin P 2016 *Phys. Chem. Chem. Phys.* **18** 27432–41
[29] Artyukh A A and Chernozatonskii L A 2019 *JETP Lett.* **109** 472–7
[30] Dong B, Sun W, Liu D and Ma N 2020 *Physica* B **577** 411824
[31] Prabhakar S and Melnik R 2019 *Physica* E **114** 113648
[32] Lyapkosova O S and Lebedev N G 2012 *Phys. Solid State* **54** 1501
[33] Lebedeva O S and Lebedev N G 2014 *Nauchno-tehnicheskie vedomosti SPbGPU. Serija 'Fiziko-matematicheskie nauki' [St. Petersburg State Polytechnical University Journal. Physics and Mathematics]* vol 189 p 26 [in Russian]
[34] Lebedeva O S and Lebedev N G 2014 *Nauchno-tehnicheskie vedomosti SPbGPU [St. Petersburg State Polytechnical University Journal]* vol 195 p 149 [in Russian]
[35] Lebedeva O S and Lebedev N G 2014 *Russ. J. Phys. Chem.* B **8** 745
[36] Lebedeva O S, Lebedev N G and Lyapkosova I A 2018 *Math. Phys. Comput. Simul.* **21** 53
[37] Landau L D and Lifshitz E M 1981 *Theory of Elasticity* 2nd edn vol 7 (*Course of Theoretical Physics* vol 7) (Oxford: Pergamon)
[38] Izyumov Yu A, Chashchin N I and Alekseev D S 2006 *Theory of Strongly Correlated Systems: Method of Generating Functional* (Moscow: Regular and Chaotic Dynamics) 384p [in Russian]
[39] Stepanov N F 2001 *Quantum Mechanics and Quantum Chemistry* (Moscow: Mir) 519p [in Russian]
[40] Bakhvalov N S 1975 *Numerical Methods* (Moscow: Nauka) 632p [in Russian]
[41] Kvasnikov I A 2005 *Termodinamika i statisticheskaja fizika. Vol 4: Kvantovaja statistika [Thermodynamics and statistical physics. Vol. 4: Quantum Statistics]* (Moscow: KomKniga Publ.) 352p [in Russian]
[42] Son Y W, Cohen M L and Louie S G 2006 *Phys. Rev. Lett.* **97** 216803
[43] Han M Y, Oezyilmaz B, Zhang Y and Kim Ph 2007 *Phys. Rev. Lett.* **98** 206805
[44] Li X, Wang X, Zhang L, Lee S and Dai H 2008 *Science* **319** 1229–32